19th AIAA Computational Fluid Dynamics
22 - 25 June 2009, San Antonio, Texas

AIAA 2009-3655

Improvement of weighted essentially non-oscillatory schemes near discontinuities

Yiqing Shen* Gecheng Zha†
Dept. of Mechanical and Aerospace Engineering
University of Miami
Coral Gables, Florida 33124
E-mail: yqshen@miami.edu, gzha@miami.edu

Abstract

In this article, we analyze the fifth-order weighted essentially non-oscillatory(WENO-5) scheme and show that, at a transition point from smooth region to a discontinuity point or vice versa, the accuracy order of WENO-5 is decreased. A new method is proposed to overcome this drawback by introducing 4th-order fluxes combined with high order smoothness indicator. Numerical examples show that the new method is more accurate near discontinuities.

1 Introduction

The WENO scheme concept was firstly proposed by Liu et al[1] and then improved by Jiang and Shu[2]. WENO schemes are based on ENO (essentially non-oscillatory) schemes[3, 4], but use a convex combination of all candidate stencils instead of the smoothest one in the ENO schemes. The WENO schemes achieve high order accuracy in smooth regions with more compact stencil and have better convergence due to the smoother numerical flux used.

Jiang and Shu[2] analyze and modify the 5th order WENO scheme proposed by Liu et al[1] and suggest a new way of measuring the smoothness of a numerical solution. Thus a WENO scheme with the optimal $(2r-1)$th order accuracy rather than $(r+1)$th order is obtained. Henrick et al[5] pointed out that the original smoothness indicators of Jiang and Shu fail to improving the accuracy order of WENO scheme at a critical point, where the first derivatives is zero. A mapping function is proposed by Henrick et al[5] to obtain the optimal order near critical points. Borges et al[6] devised a new set of WENO weights that satisfies the necessary and sufficient conditions for fifth-order convergence proposed by Henrick et al[5] and enhances the accuracy at critical points. A class of higher than 5th order weighted essentially non-oscillatory schemes are designed by Balsara and Shu in [7]. Wang and Chen [8] proposed optimized WENO schemes for linear waves with discontinuity. Martin et al[9] proposed a symmetric WENO method by means of a new candidate stencil, the new schemes are $2r$th-order accurate and symmetric, and less dissipative than Jiang and Shu's scheme.

The above mentioned WENO schemes are designed to have $(2r-1)$th or $2r$th[9] order of accuracy in the smooth regions directly from rth ENO scheme. For a solution containing discontinuity, these methods can not obtain the optimal accuracy near the discontinuity points. Shen et al[10] indicate that the smoothness

* Research Scientist, AIAA Member
† Associate Professor, AIAA Senior Member

indicator IS_k of Jiang and Shu's WENO scheme does not satisfy the condition $\beta_k = D(1 + O(\Delta x^2))$ at the critical point ($f_i' = 0$), and proposed a step-by-step reconstruction to avoid the strict condition.

In this article, the analysis of the fifth-order WENO(WENO-5) scheme indicates that, at a transition point from smooth region to a discontinuity point or vice versa, the accuracy order of WENO-5 is decreased. Fourth-order reconstructions are introduced and combined with the higher order smoothness indicators to overcome this drawback. Numerical examples show that this new method is more accurate near discontinuities.

2 Weighted essentially non-oscillatory schemes

For the hyperbolic conservation law in the form

$$\frac{\partial u}{\partial t} + \frac{\partial f}{\partial x} = 0 \tag{1}$$

the semi-discretization form can be written as

$$\frac{du_i(t)}{dt} = -\frac{1}{\Delta x}(h_{i+\frac{1}{2}} - h_{i-\frac{1}{2}}) \tag{2}$$

The fluxes of classical fifth-order WENO scheme are built through the convex combination of interpolated values $\hat{f}^k(x_{i\pm\frac{1}{2}})$,

$$h_{i+\frac{1}{2}} = \sum_{k=0}^{2} \omega_k \hat{f}^k(x_{i+\frac{1}{2}}) \tag{3}$$

in which $\hat{f}^k(x)$ is the third degree polynomial, defined as

$$\hat{f}^k_{i+\frac{1}{2}} = \hat{f}^k(x_{i+\frac{1}{2}}) = \sum_{j=0}^{2} c_{kj} f_{i-k+j}, \quad i = 0, \cdots, N \tag{4}$$

The weights ω_k are defined as

$$\omega_k = \frac{\alpha_k}{\sum_{l=0}^{2} \alpha_l}, \quad \alpha_k = \frac{d_k}{(\beta_k + \varepsilon)^p} \tag{5}$$

The smoothness indicators β_k are given by[2]

$$\beta_k = \sum_{l=1}^{2} \Delta x^{2l-1} \int_{x_{i-\frac{1}{2}}}^{x_{i+\frac{1}{2}}} (\frac{d^l}{dx^l} \hat{f}^k(x))^2 dx \tag{6}$$

Taylor expansion of (6) gives

$$\begin{array}{l} \beta_0 = \frac{13}{12}(f_{i-2} - 2f_{i-1} + f_i)^2 + \frac{1}{4}(f_{i-2} - 4f_{i-1} + 3f_i)^2 \\ \beta_1 = \frac{13}{12}(f_{i-1} - 2f_i + f_{i+1})^2 + \frac{1}{4}(f_{i-1} - f_{i+1})^2 \\ \beta_2 = \frac{13}{12}(f_i - 2f_{i+1} + f_{i+2})^2 + \frac{1}{4}(3f_i - 4f_{i+1} + f_{i+2})^2 \end{array} \tag{7}$$

Henrick et al[5] shown that if β_k satisfy $\beta_k = D(1 + O(\Delta x^s))$, then the weights ω_k satisfy $\omega_k = d_k + O(\Delta x^s)$, where D is some non-zero quantity independent of k. And the necessary and sufficient conditions for fifth-order convergence in (2) are given as[5]:

Table 1: Coefficients c_{kj} and d_k

	c_{kj}			d_k
k	j=0	j=1	j=2	
0	1/3	-7/6	11/6	1/10
1	-1/6	5/6	1/3	6/10
2	1/3	5/6	-1/6	3/10

$$\sum_{k=0}^{2}(\omega_k^{\pm} - d_k) = O(\Delta x^6) \tag{8}$$

$$\sum_{k=0}^{2} A_k(\omega^{+} - \omega^{-}) = O(\Delta x^3) \tag{9}$$

$$\omega_k^{\pm} - d_k = O(\Delta x^2) \tag{10}$$

If $f_i' = 0$, then Eq.(7) gives $\beta_k = D(1+O(\Delta x))$ and $\omega_k = d_k + O(\Delta x)$, this will degrade the convergence accuracy of the scheme. Shen et al [10] proposed a step-by-step reconstruction can reduce (10) as $\omega_k^{\pm} - d_k = O(\Delta x)$. Henrick et al[5] proposed a mapping function to increase the approximation of ω_k to the ideal weights d_k.

Borges et al [6] introduced the absolute difference between β_0 and β_2 to devise a new set of WENO weights that satisfies the necessary and sufficient conditions for fifth-order convergence. The new smoothness indicators β_k^z defined by Borges et al [6] are

$$\beta_k^z = \frac{\beta_k + \varepsilon}{\beta_k + \tau_5 + \varepsilon}, \quad k = 0, 1, 2 \tag{11}$$

and the new WENO weights ω_k^z are

$$\omega_k^z = \frac{\alpha_k^z}{\sum_{l=0}^{2}\alpha_l^z}, \quad \alpha_k^z = \frac{d_k}{\beta_k^z} = d_k(1 + (\frac{\tau_5}{\beta_k + \varepsilon})^q), \quad k = 0, 1, 2 \tag{12}$$

where

$$\tau_5 = |\beta_0 - \beta_2| \tag{13}$$

If $f_i' \neq 0$, then Eq.(12) with $q = 1$ gives $\omega_k - d_k = O(\Delta x^3)$; if $f_i' = 0$, then (12) with $q = 2$ gives $\omega_k - d_k = O(\Delta x^2)$.

The parameter ε is used to avoid the division by zero ($\varepsilon = 10^{-6}$ is used in [2] and $\varepsilon = 10^{-40}$ is used in [6]) and p and q are chosen to increase the difference of scales of distinct weights at non-smooth parts of the solution. The coefficients c_{kj} and d_k are list in Table 1.

The study of Borges et al [6] shows that the new smoothness indicators β_k^z have higher order accuracy than the original β_k of Jiang and Shu's[2], the resulted WENO scheme (WENO-Z) has less dissipation and higher resolution than Jiang and Shu's WENO (WENO-JS).

Fifth-order WENO schemes can capture shock wave and have fifth-order accuracy in smooth regions. However, because the WENO scheme is constructed directly from rth-order interpolation to $(2r-1)$th-order, the accuracy is reduced at the transition point from smooth region to discontinuous point and vice versa. In order to demonstrate this conclusion, Fig. 1 is taken as an example.

At point $(i-1)$, the stencil $S^5_{(i-1)-1/2}$ is

$$S^5_{(i-1)-1/2} = \{x_{i-4}, x_{i-3}, x_{i-2}, x_{i-1}, x_i\} \tag{14}$$

and it is a smooth stencil, $h_{(i-1)-1/2}$ is obtained by the process of WENO-Z or WENO-JS as a fifth-order flux.

However, for

$$S^5_{(i-1)+1/2} = \{x_{i-3}, x_{i-2}, x_{i-1}, x_i, x_{i+1}\} \tag{15}$$

There is a discontinuity at stencil $S^3_2 = \{x_{i-1}, x_i, x_{i+1}\}$, so

$$\beta_2 >> \beta_0, \beta_1 \tag{16}$$

no matter whether WENO-Z or WENO-JS is used. For calculating the flux $h_{(i-1)+1/2}$, from Eq. (5) or (12), it is easy to find

$$\omega_0 \to \frac{1}{7},\ \omega_1 \to \frac{6}{7},\ \omega_2 \to 0 \tag{17}$$

The case at point $(i+3)$ is similar to the point $i-1$. $S^5_{(i+3)-1/2}$ contains a discontinuity at stencil $S^3_0 = \{x_i, x_{i+1}, x_{i+2}\}$, while $S^5_{(i+3)+1/2} = \{x_{i+1}, x_{i+2}, x_{i+3}, x_{i+4}, x_{i+5}\}$ is a smooth stencil. For the flux $h_{(i+3)-1/2}$,

$$\omega_0 \to 0,\ \omega_1 \to \frac{2}{3},\ \omega_2 \to \frac{1}{3} \tag{18}$$

Let us look at a numerical example of a discontinuous function

$$u(0,x) = f(x) = \begin{cases} -sin(\pi x) - \frac{1}{2}x^3, & -1 < x \le 0, \\ -sin(\pi x) - \frac{1}{2}x^3 + 1, & 0 < x \le 1, \end{cases} \tag{19}$$

consisting of a piecewise sine function with a jump discontinuity at $x_i = 0$. The weights calculated by WENO-Z scheme (eq.(12)) is shown in Fig. 2, it demonstrates the previous conclusion. For the flux $h_{(i-1)+1/2}$, $\omega_0 \approx \frac{1}{7}$ (point A), $\omega_1 \approx \frac{6}{7}$(point B). For $h_{(i+3)-1/2}$, $\omega_1 \approx \frac{2}{3}$ (point D), $\omega_1 \approx \frac{1}{3}$(point C).

Under the case of $\Delta x \to 0$, there are

$$h_{(i-1)-\frac{1}{2}} = \frac{1}{30}f_{i-4} - \frac{13}{60}f_{i-3} + \frac{47}{60}f_{i-2} + \frac{9}{20}f_{i-1} - \frac{1}{20}f_i \tag{20}$$

and

$$h_{(i-1)+\frac{1}{2}} = \frac{1}{20}f_{i-3} - \frac{13}{42}f_{i-2} + \frac{41}{42}f_{i-1} + \frac{2}{7}f_i \tag{21}$$

Applying Taylor series expansion, there is

$$\frac{1}{\Delta x}(h_{(i-1)+\frac{1}{2}} - h_{(i-1)-\frac{1}{2}}) = f'_{i-1} + O(\Delta x^3) \tag{22}$$

The accuracy of the downstream point $(i+3)$ can be analyzed similarly.

That is, at the points (continuous point) immediately upstream or downstream of a discontinuity, the fifth-order WENO scheme only gives third-order accuracy.

3 The New Method

In this section, a new method is proposed to overcome the drawback of WENO mentioned above. The method combines the idea of the step-by-step construction of a higher order WENO scheme[10] and the properties of τ_5 introduced by Borges etal[6]. For completeness, two important properties of τ_5 are listed here:

(1) If the stencil S^5 does not contain discontinuities, then $\tau_5 << \beta_k$ for $k = 0, 1, 2$;

(2) if the solution is continuous at some of the stencil S_i^3, but discontinuous in the whole stencil S^5, then $\beta_i << \tau_5$.

The new method can be described using the sketch of Fig. 3.

First, the stencils S_0^4 and S_1^4 are defined as

$$S_0^4 = S_0^3 \cup S_1^3 = \{x_{i-2}, x_{i-1}, x_i, x_{i+1}\} \tag{23}$$

$$S_1^4 = S_1^3 \cup S_2^3 = \{x_{i-1}, x_i, x_{i+1}, x_{i+2}\} \tag{24}$$

Following the definition of τ_5 in Ref. [6], we define τ_4^0 and τ_4^1 as following,

$$\tau_4^0 = |\beta_0 - \beta_1| \tag{25}$$

$$\tau_4^1 = |\beta_1 - \beta_2| \tag{26}$$

τ_4^0 and τ_4^1 have the same properties as τ_5,

(1) If S_l^4 $(l = 0, 1)$ does not contain discontinuities, then $\tau_4^l << \beta_{l+k}$ for $k = 0, 1$;

(2) if the solution is continuous at S_{l+i}^3, but discontinuous in the whole S_l^4, then $\beta_{l+i} << \tau_4^l$.

From the two properties, the following conclusions can be drawn:

(1) if $\tau_4^0 \leq min(\beta_0, \beta_1, \beta_2)$ and $\tau_4^1 > min(\beta_0, \beta_1, \beta_2)$, then there is a discontinuity at S_2^3, i.e. within (x_{i+1}, x_{i+2});

(2) if $\tau_4^0 > min(\beta_0, \beta_1, \beta_2)$ and $\tau_4^1 \leq min(\beta_0, \beta_1, \beta_2)$, then there is a discontinuity at S_0^3, i.e. within (x_{i-2}, x_{i-1}).

Therefore, the new method is constructed as

$$h_{i+\frac{1}{2}} = \begin{cases} h_0^4, \ if \ \tau_4^0 \leq min(\beta_0, \beta_1, \beta_2) \ and \ \tau_4^1 > min(\beta_0, \beta_1, \beta_2), \\ h_1^4, \ if \ \tau_4^0 > min(\beta_0, \beta_1, \beta_2) \ and \ \tau_4^1 \leq min(\beta_0, \beta_1, \beta_2), \\ h^{WENO-Z}, \ otherwise \end{cases} \tag{27}$$

where

$$h_0^4 = C_0^{4,0} \hat{f}_{i+1/2}^0 + C_1^{4,0} \hat{f}_{i+1/2}^1, \quad h_1^4 = C_0^{4,1} \hat{f}_{i+1/2}^1 + C_1^{4,1} \hat{f}_{i+1/2}^2 \tag{28}$$

and

$$C_0^{4,0} = \frac{1}{4}, \ C_1^{4,0} = \frac{3}{4}; \quad C_0^{4,1} = \frac{1}{2}, \ C_1^{4,1} = \frac{1}{2}$$

That is

$$h_0^4 = \frac{1}{12} f_{i-2} - \frac{5}{12} f_{i-1} + \frac{13}{12} f_i + \frac{1}{4} f_{i+1}$$

$$h_1^4 = -\frac{1}{12} f_{i-1} + \frac{7}{12} f_i + \frac{7}{12} f_{i+1} - \frac{1}{12} f_{i+2}$$

Again, the point $(i-1)$ in Fig. 1 is taken as an example, $S_0^4|_{i-1/2} = \{x_{i-3}, x_{i-2}, x_{i-1}, x_i\}$ is a smooth stencil, according to the properties of τ_4^l, there is

$$\tau_4^0 < min(\beta_0, \beta_1, \beta_2) \ \ and \ \ \tau_4^1 >> min(\beta_0, \beta_1, \beta_2)$$

so

$$h_{(i-1)+1/2} = h_0^4 = \frac{1}{12} f_{i-3} - \frac{5}{12} f_{i-2} + \frac{13}{12} f_{i-1} + \frac{1}{4} f_i$$

Table 2: Results and errors

Point	x_i	$f'(x_i)$	f'_i(WENO-Z)	f'_i(present)	error(WENO-Z)	error(present)
	-0.2000	-.26016E+01	-.26016E+01	-.26016E+01	0.31953E-05	0.31953E-05
	-0.1500	-.28329E+01	-.28329E+01	-.28329E+01	0.25566E-05	0.25566E-05
	-0.1000	-.30028E+01	-.30028E+01	-.30028E+01	0.18554E-05	0.18554E-05
	-0.0500	-.31067E+01	-.31048E+01	-.31066E+01	**0.19045E-02**	**0.95956E-04**
N=40	0.0000	-.31416E+01	-.31343E+01	-.31325E+01	0.72982E-02	0.91067E-02
	0.0500	-.31067E+01	0.16883E+02	0.16883E+02	0.19989E+02	0.19989E+02
	0.1000	-.30028E+01	-.29997E+01	-.30012E+01	0.31294E-02	0.15856E-02
	0.1500	-.28329E+01	-.28346E+01	-.28331E+01	**0.16706E-02**	**0.12686E-03**
	0.2000	-.26016E+01	-.26016E+01	-.26016E+01	0.26522E-05	0.26522E-05
	-0.1000	-.30028E+01	-.30028E+01	-.30028E+01	0.53282E-07	0.53282E-07
	-0.0750	-.30632E+01	-.30632E+01	-.30632E+01	0.41587E-07	0.41587E-07
	-0.0500	-.31067E+01	-.31067E+01	-.31067E+01	0.29636E-07	0.29636E-07
	-0.0250	-.31328E+01	-.31323E+01	-.31328E+01	**0.52653E-03**	**0.59822E-05**
N=80	0.0000	-.31416E+01	-.31436E+01	-.31431E+01	0.20075E-02	0.14870E-02
	0.0250	-.31328E+01	0.36868E+02	0.36868E+02	0.40000E+02	0.40000E+02
	0.0500	-.31067E+01	-.31052E+01	-.31057E+01	0.14201E-02	0.99143E-03
	0.0750	-.30632E+01	-.30637E+01	-.30632E+01	**0.43659E-03**	**0.79597E-05**
	0.1000	-.30028E+01	-.30028E+01	-.30028E+01	0.43276E-07	0.43276E-07
	-0.0500	-.31067E+01	-.31067E+01	-.31067E+01	0.84590E-09	0.84590E-09
	-0.0375	-.31219E+01	-.31219E+01	-.31219E+01	0.65623E-09	0.65623E-09
	-0.0250	-.31328E+01	-.31328E+01	-.31328E+01	0.46551E-09	0.46551E-09
	-0.0125	-.31394E+01	-.31393E+01	-.31394E+01	**0.14246E-03**	**0.37364E-06**
N=160	0.0000	-.31416E+01	-.31425E+01	-.31423E+01	0.89829E-03	0.75621E-03
	0.0125	-.31394E+01	0.76861E+02	0.76861E+02	0.80000E+02	0.80000E+02
	0.0250	-.31328E+01	-.31324E+01	-.31325E+01	0.42399E-03	0.31005E-03
	0.0375	-.31219E+01	-.31220E+01	-.31219E+01	**0.11444E-03**	**0.49793E-06**
	0.0500	-.31067E+01	-.31067E+01	-.31067E+01	0.68340E-09	0.68340E-09

Meanwhile, $S^5_{i-3/2}$ is a smooth stencil, $h_{(i-1)-1/2}$ keeps the fifth-order flux $h^{WENO-Z}_{(i-1)-1/2}$ (Eq.(20)). Hence, applying Taylor series expansion, there is

$$\frac{1}{\Delta x}(h_{(i-1)+\frac{1}{2}} - h_{(i-1)-\frac{1}{2}}) = f'_{i-1} + O(\Delta x^4) \tag{29}$$

Compared with the accuracy of the original WENO-Z or WENO-JS scheme (Eq. (22)), the new method improves one accuracy order at the point right next to the discontinuity $(i-1)$.

Table 2 gives the comparison of values and errors of WENO-Z scheme and the present method of first-order derivative of $f(x)$(Eq. 19) near the discontinuity points. For this case, $x_i = 0$ and the next point x_{i+1} are the discontinuity points. At points x_{i-1} and x_{i+3}, the present method is clearly more accurate than WENO-Z scheme.

3.1 Numerical Examples

In this paper, the 4th order Runge-Kutta-type method[11] is used for the time integration.

Table 3: Accuracy on $u_t + u_x = 0$ with $u_0(x) = sin(\pi x)$, t=1

Scheme	N	L_∞ error	L_∞ order	L_1 error	L_1 order
WENO-Z	40	0.315356E-03	—-	0.198512E-03	—-
	80	0.994903E-05	4.986	0.628679E-05	4.981
	160	0.312476E-06	4.993	0.197921E-06	4.989
	320	0.977606E-08	4.998	0.620618E-08	4.995
	640	0.305593E-09	5.000	0.194260E-09	4.998
present	40	0.315356E-03	—-	0.198512E-03	—-
	80	0.994903E-05	4.986	0.628679E-05	4.981
	160	0.312476E-06	4.993	0.197921E-06	4.989
	320	0.977606E-08	4.998	0.620618E-08	4.995
	640	0.305593E-09	5.000	0.194260E-09	4.998

3.1.1 Linear transport equation

The linear transport equation is used to test the accuracy of WENO schemes.

$$\frac{\partial u}{\partial t} + \frac{\partial u}{\partial x} = 0, \ -1 < x < 1 \tag{30}$$
$$u(x,0) = u_0(x), \ periodic$$

(1) Initial solution $u_0(x) = sin(2\pi x)$

Table 3 gives the errors and accuracy order. It can be seen that, for the smooth solution, the present scheme obtains the same results and accuracy order as the WENO-Z scheme.

(2) Initial solution

$$u(0,x) = f(x) = \begin{cases} -sin(\pi x) - \frac{1}{2}x^3, & -1 < x \le 0, \\ -sin(\pi x) - \frac{1}{2}x^3 + 1, & 0 < x \le 1, \end{cases} \tag{31}$$

Fig. 4 shows the numerical solutions at $t = 10$. It can be seen that, near the discontinuity, the present method obtains more accurate solution.

(3) Initial solution

$$u_0(x) = \begin{cases} -xsin(3\pi x^2/2), & -1 \le x < -1/3 \\ |sin(2\pi x)|, & -1/3 \le x \le 1/3 \\ 2x - 1 - sin(3\pi x)/6, & otherwise \end{cases} \tag{32}$$

Fig. 5 shows the numerical solutions at $t = 6$. Again, it can be seen present method is more accurate.

(4) Initial solution

$$u_0(x) = \begin{cases} \frac{1}{6}(G(x,\beta,z-\delta) + G(x,\beta,z+\delta) + 4G(x,\beta,z)), & -0.8 \le x \le -0.6, \\ 1, & -0.4 \le x \le -0.2, \\ 1 - |10(x-0.1)|, & 0 \le x \le 0.2, \\ \frac{1}{6}(F(x,\alpha,\alpha-\delta) + F(x,\alpha,\alpha+\delta) + 4F(x,\alpha,a)), & 0.4 \le x \le 0.6, \\ 0, & otherwise \end{cases} \tag{33}$$

As in Ref.[2], the constants for this case are taken as $a = 0.5$, $z = -0.7$, $\delta = 0.005$, $\alpha = 10$, and $\beta = log2/36\delta^2$. The solution contains a smooth combination of Gaussians, a square wave, a sharp triangle wave, and a half ellipse.

The results at $t = 8$ with 200 grid points are shown in Fig. 6. From the zoomed plots in Figure 7, it can be seen that, present method can improve the accuracy not only near the discontinuities, but also for the peak of the half ellipse wave.

3.1.2 Nonlinear Transport Equation

The nonlinear transport equation can be written as

$$\frac{\partial u}{\partial t} + u\frac{\partial u}{\partial x} = 0,\ 0 \le x \le 2\pi$$

with initial and boundary conditions

$$u_0(x) = 0.3 + 0.7sin(x),\ 0 \le x \le 2\pi,\ periodic$$

The Lax-Friedrichs splitting method is used, in which $f^{\pm} = \frac{1}{2}(f(u) \pm au)$, $f(u) = \frac{1}{2}u^2$, and $a = max_u|f'(u)|$. Fig. 8 shows the results at $t = 2$ with grid number of $N = 80$. It can be seen that, near the shock, the solution calculated by the present scheme is closer to the discontinuous points than those of WENO-Z scheme.

3.1.3 1D Shock Wave Tube, Sod Problem

To examine the new scheme for nonlinear equations, the one-dimensional Euler equations are solved for the 1D shock tube problem.

1D Euler equations:

$$\frac{\partial \mathbf{U}}{\partial t} + \frac{\partial \mathbf{F}}{\partial x} = 0 \tag{34}$$

where

$$\mathbf{U} = \begin{bmatrix} \rho \\ \rho u \\ \rho e \end{bmatrix}\ \mathbf{F} = \begin{bmatrix} \rho u \\ \rho u^2 + p \\ u(\rho e + p) \end{bmatrix},\ p = (\gamma - 1)(\rho e - \rho u^2/2),\ \gamma = 1.4.$$

The initial condition is

$$(\rho, u, p) = \begin{cases} (1.0, 0.0, 1.0), & x \le 7.5, \\ (0.125, 0.0, 0.1), & x > 7.5. \end{cases} \tag{35}$$

In this case, the Roe's Riemann solver is used. The grid points is $N = 200$. Fig. 9 give the density distribution. Both the WENO-Z and present schemes capture the shock very well. The present scheme improves the resolution near the discontinuities.

3.1.4 1D Shock Wave Tube, Shu-Osher Problem

This problem is governed by the one-dimensional Euler equations (34) with following initial condition:

$$(\rho, u, p) = \begin{cases} (3.857143, 2.629369, 10.3333), & when\ x < -4, \\ (1 + \varepsilon sin(5x), 0.0, 1.0), & when\ x \ge -4. \end{cases} \tag{36}$$

where, $\varepsilon = 0.2$. This case represents a Mach 3 shock wave interacting with a sine entropy wave[4]. The results at time $t = 1.8$ are plotted in Figs. 10. The "exact" solutions are the numerical solutions of the original WENO-5 scheme with grid points of $N = 8000$. For this case, it can be seen that the present WENO scheme resolves the profile better than the WENO-Z scheme.

3.1.5 Two-dimensional Linear Conservation Equation with Variable Coefficients

To test the multidimensional problems, the 2D linear conservation equation with variable coefficients is solved. The governing equation is

$$\frac{\partial u}{\partial t} + \frac{\partial(-yu)}{\partial x} + \frac{\partial(xu)}{\partial y} = 0,\ -1 \le x, y \le 1. \tag{37}$$

and the periodic boundary conditions are used. The initial condition is chosen as the characteristic function of a circle with radius 0.5 as shown in Fig. 11. The problem represents a solid body rotation[12, 13]. The results at $t = 2$ in a 100×100 points grid are shown in Fig. 12. Note that in Fig. 12, the exact solution at $x = -0.52$ is $u(-0.52, y) = 0$. It can be seen that the present scheme obtains more accurate solution than the WENO-Z scheme, especially at the location $x = -0.48$ and $x = -0.52$.

3.1.6 Two-dimensional Shock Vortex Interaction

A two-dimensional shock vortex interaction problem is solved to further demonstrate the high resolution of the present scheme. The two-dimensional Euler equations are solved for this problem:

$$\frac{\partial \mathbf{U}}{\partial t} + \frac{\partial \mathbf{E}}{\partial x} + \frac{\partial \mathbf{F}}{\partial y} = 0 \tag{38}$$

where

$$\mathbf{U} = \begin{bmatrix} \rho \\ \rho u \\ \rho v \\ \rho e \end{bmatrix}, \mathbf{E} = \begin{bmatrix} \rho u \\ \rho u^2 + p \\ \rho uv \\ u(\rho e + p) \end{bmatrix}, \mathbf{F} = \begin{bmatrix} \rho v \\ \rho uv \\ \rho v^2 + p \\ v(\rho e + p) \end{bmatrix},$$

$p = (\gamma - 1)(\rho e - \rho(u^2 + v^2)/2)$, $\gamma = 1.4$.

The problem is taken from Ref.[2]. It describes the interaction between a stationary shock and a vortex. The computational domain is taken to be $[0, 2] \times [0, 1]$. A stationary Mach 1.1 shock is positioned at $x = 0.5$ and normal to the x-axis. Its left state is $(\rho, u, v, p) = (1, 1.1\sqrt{\gamma}, 0, 1)$. A small vortex is superimposed to the flow on the left of the shock and is centered at $(x_c, y_c) = (0.25, 0.5)$. The vortex is described as a perturbation to the velocity (u, v), temperature $(T = p/\rho)$, and entropy $(S = ln(p/\rho^\gamma))$ of the mean flow and denoted by the tilde values:

$$\tilde{u} = \varepsilon\tau e^{a(1-\tau^2)} sin\theta$$

$$\tilde{v} = -\varepsilon\tau e^{a(1-\tau^2)} cos\theta$$

$$\tilde{T} = -\frac{(\gamma - 1)\varepsilon^2 e^{2a(1-\gamma^2)}}{4a\gamma}$$

$$\tilde{S} = 0$$

where $\tau = r/r_c$ and $r = \sqrt{(x - x_c)^2 + (y - y_c)^2}$, ε indicates the strength of the vortex, a controls the decay rate of the vortex, and r_c is the critical radius for which the vortex has the maximum strength. As in the Refs. [2, 14], $\varepsilon = 0.3$, $r_c = 0.05$, and $a = 0.204$ are adopted in this paper. The uniform grid of 251×101 is used. The time step is taken as follows[8]:

$$\Delta t = \delta \Delta_x \Delta_y,\ with\ \delta_x = \frac{\Delta x}{max_{i,j}(|u_{i,j}| + c_{i,j})},\ \delta_y = \frac{\Delta y}{max_{i,j}(|v_{i,j}| + c_{i,j})} \tag{39}$$

Fig. 13 is the pressure contours at $t = 0.60$. Figs. 14 and 15 are the comparisons of the pressure between the present and the original scheme along the center line at $y = 0.5$. In order to show the accuracy of

the new scheme, the results obtained by the WENO-Z scheme with a mesh of 1001×401 is also given. With the same mesh density, the new scheme obtains more accurate results than the original scheme. Fig. 14 also shows that the new scheme has the sharper shock profile. Fig. 15 indicates that the new scheme achieves lower vortex core pressure due to lower numerical dissipation.

4 Conclusions

This paper has analyzed the reason that traditional weighted essentially non-oscillatory(WENO) scheme reduce it's accuracy near the discontinuities. The method combined the forth-order fluxes with higher order smoothness indicator is proposed to overcome this drawback. Numerical examples show that the new method is efficient.

5 Acknowledgment

This work is partially supported by AFOSR Grant FA9550-06-1-0198 monitored by Dr Fariba Fahroo, by ARO grant 56827-RT-ISP monitored by John Schmisseur at AFOSR and Peggy A. Lacewell at ARO, and by Miami Wind^{TM} at University of Miami.

References

[1] X.D. Liu, S. Osher, and T. Chan, "Weighted essentially non-oscillatory schemes," *J.Comput.Phys.*, vol. 115, pp. 200–212, 1994.

[2] G.S. Jiang, and C.W. Shu, "Efficient implementation of weighted ENO schemes," *J.Comput.Phys.*, vol. 126, pp. 202–228, 1996.

[3] A. Harten, B. Engquist, S. Osher, and S. Chakravarthy, "Uniformly High Order Essentially Non-Oscillatory Schemes, III," *Journal of Computational Physics*, vol. 71, pp. 231–303, 1987.

[4] C.-W. Shu and O. Osher, "Efficient Implementation of Essentially Non-Oscillatory Shock Capturing Schemes, II," *Journal of Computational Physics*, vol. 83, pp. 32–78, 1989.

[5] A.K. Henrick, T.D. Aslam, J.M. Powers, "Mapped weighted essentially non-oscillatory schemes:Achiving optimal order near critical points," *J.Comput.Phys.*, vol. 208, pp. 206–227, 2005.

[6] R. Borges, M. Carmona, B. Costa and W.S. Don, "An improved weighted essentially non-oscillatory scheme for hyperbolic conservation laws," *Journal of Computational Physics*, vol. 227, pp. 3191–3211, 2008.

[7] D.S. Balsara and C.-W. Shu, "Monotonicity Preserving weighted essentially non-oscillatory schemes with increasingly high order of accuracy," *J.Comput.Phys.*, vol. 160, pp. 405–452, 2000.

[8] Z.J. Wang and R.F. Chen, "Optimized weighted essentially non-oscillatory schemes for linear waves with discontinuity," *J.Comput.Phys.*, vol. 174, pp. 381–404, 2001.

[9] M. P. Martin, E. M. Taylor, M. Wu, and V. G. Weirs, "A Bandwidth-Optimized WENO Scheme for the Direct Numerical Simulation of Compressible Turbulenc," *Journal of Computational Physics*, vol. 220, pp. 270–289, 2006.

[10] Y. Q. Shen, R. Q. Wang, and H. Z. Liao, " A fifth-order accurate weighted ENN difference scheme and its applications," *Journal of Computational Mathematics*, vol. 19, pp. 531–538, 2001.

[11] C.-W. Shu and O. Osher, "Efficient Implementation of Essentially Non-Oscillatory Shock Capturing Schemes," *Journal of Computational Physics*, vol. 77, pp. 439–471, 1988.

[12] B. Cockburn, C.W. Shu, "Nonlinearly stable compact schemes for shock calculations," *SIAM Journal on Numerical Analysis*, vol. 31, pp. 607–627, 1994.

[13] Y.Q. Shen, G.W. Yang, Z. Gao, "High-resolution finite compact difference schemes for hyperbolic conservation laws," *J.Comput.Phys.*, vol. 216, pp. 114–137, 2006.

[14] Y.Q. Shen and G.W. Yang, "Hybrid finite compact-WENO schemes for shock calculation," *International Journal for Numerical Methods in Fluids*, vol. 53, pp. 531–560, 2007.

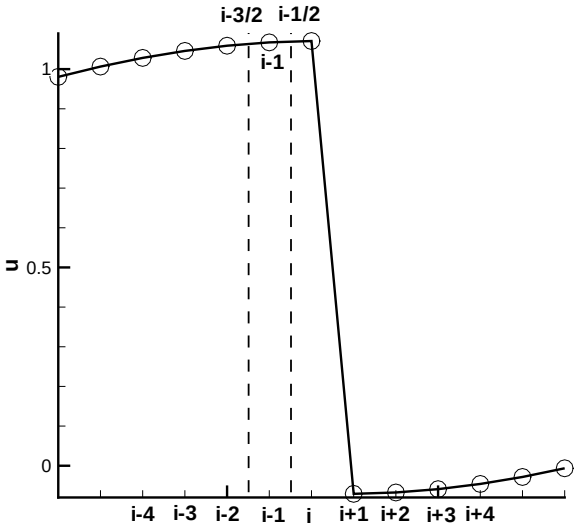

Figure 1: The sketch of transition point

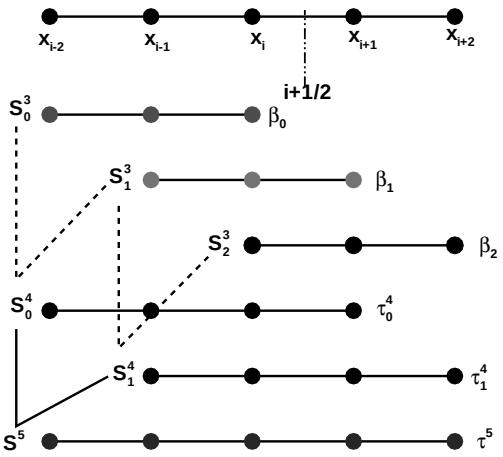

Figure 3: The sketch of reconstruction process

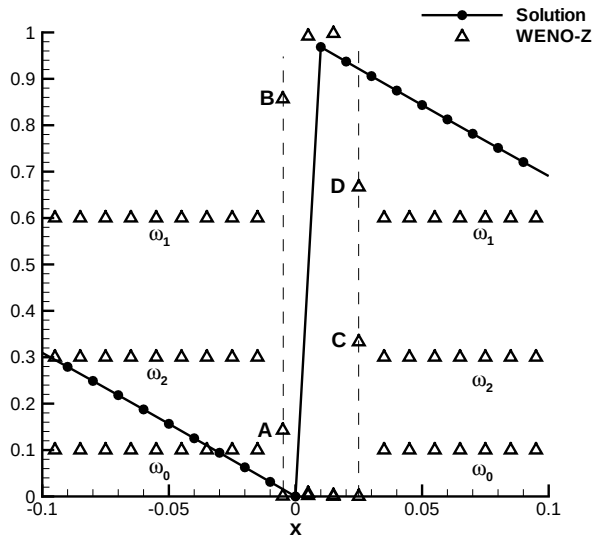

Figure 2: The distribution of weights of WENO-Z scheme

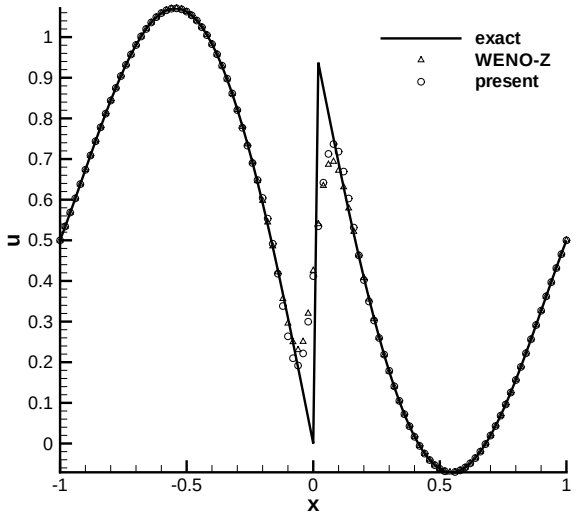

Figure 4: Numerical results, t=10

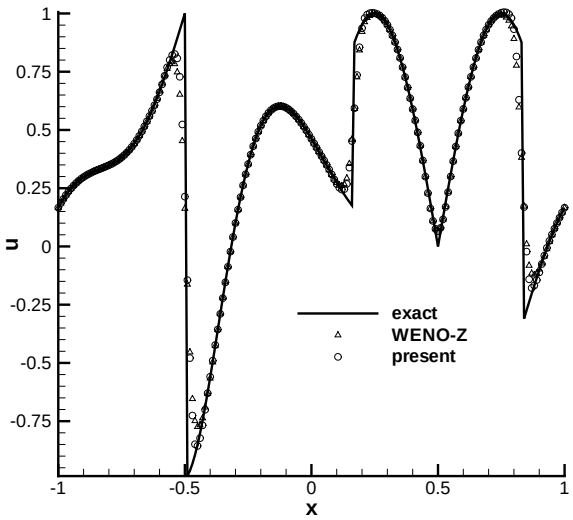

Figure 5: Numerical results, t=6

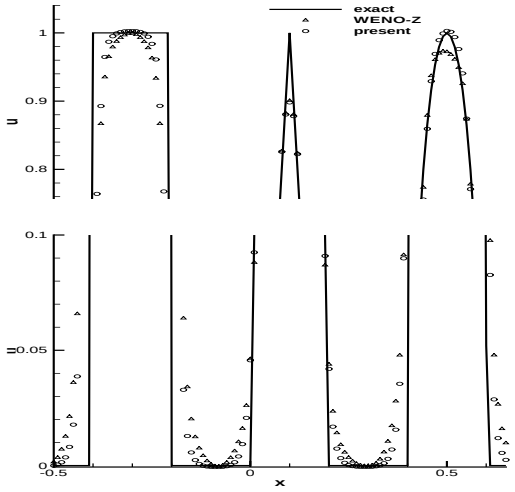

Figure 7: Locally enlarged plot of Fig. 6

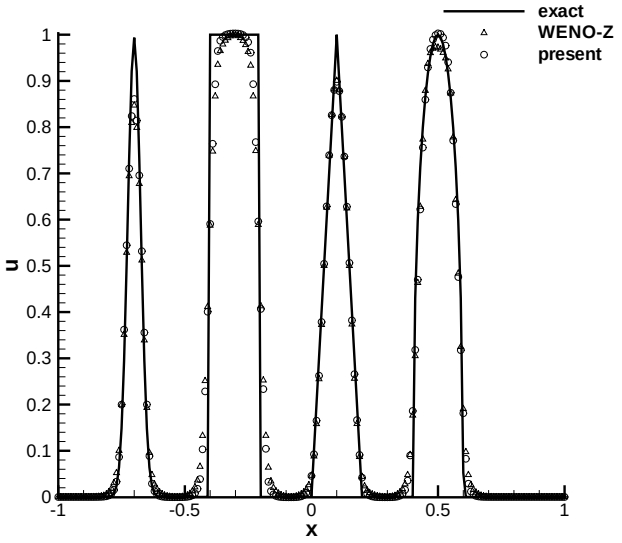

Figure 6: Numerical results, T=8

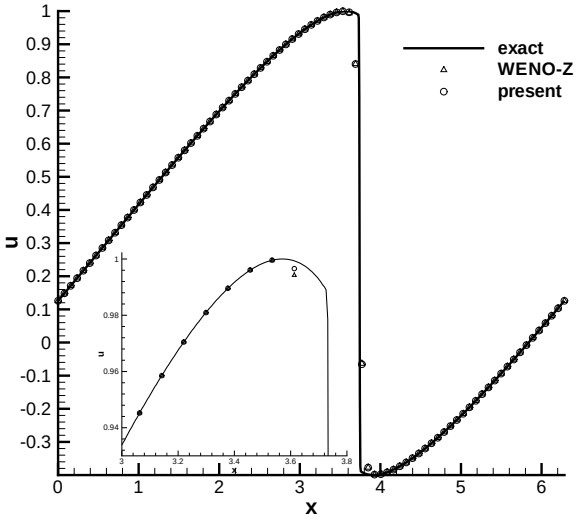

Figure 8: Numerical results, T=2

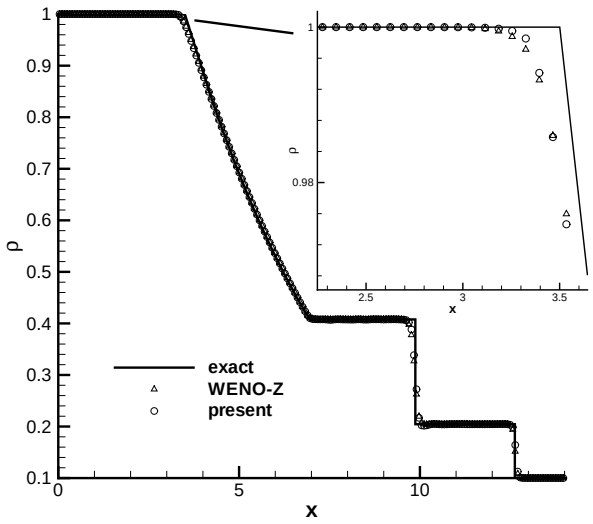

Figure 9: Density distribution, Sod problem

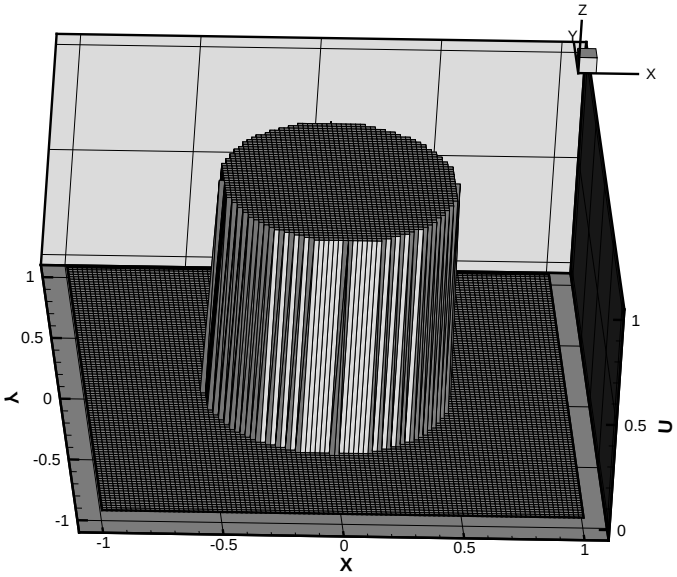

Figure 11: The initial distribution

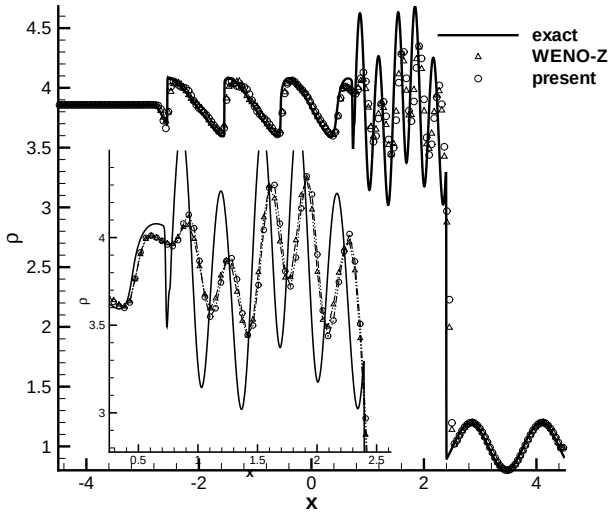

Figure 10: Density, Shu-Osher problem

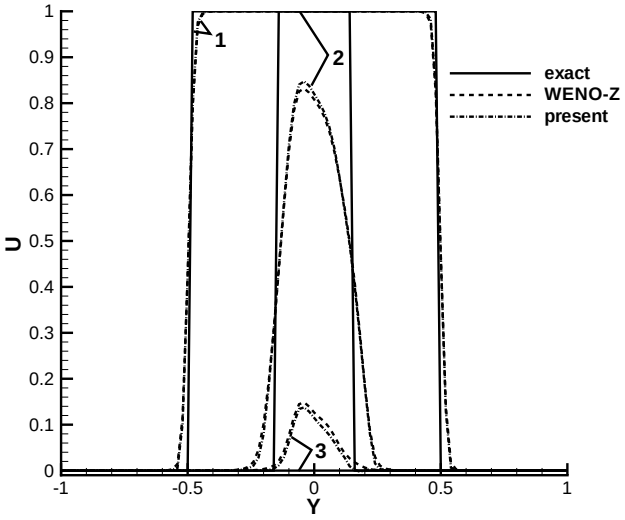

Figure 12: Comparison of results on lines. 1: $x = -0.02$; 2: $x = -0.48$; and 3: $x = -0.52$

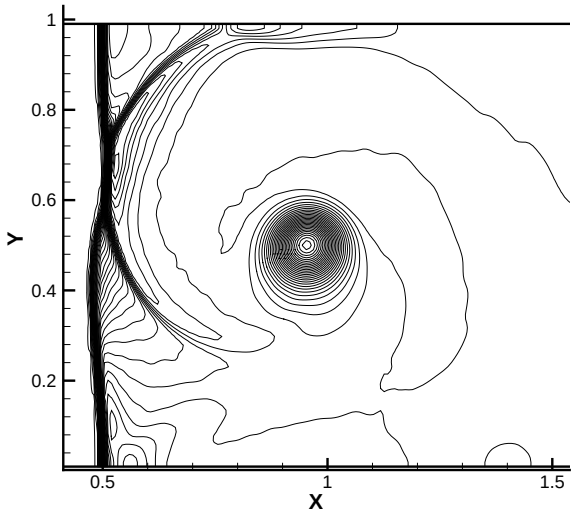

Figure 13: The pressure contours of present scheme, $t = 0.60$

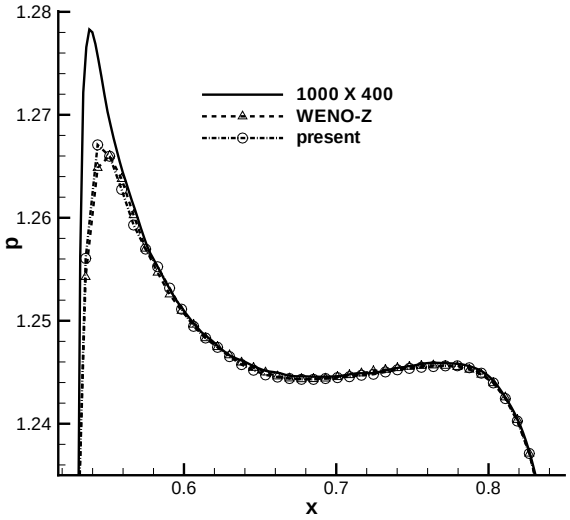

Figure 14: Comparison of pressure at the central line downstream the shock, $t = 0.60$

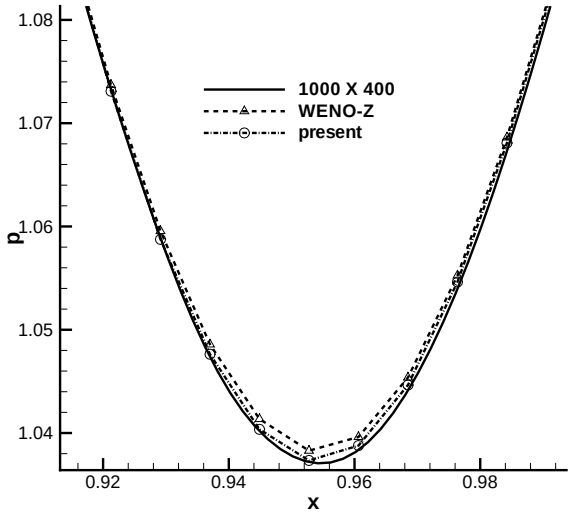

Figure 15: Comparison of pressure at the central line cross the vortex, $t = 0.60$